

Reverse segregation in dense granular flow through narrow vertical channel

Bhanjan Debnath ^{*1}

¹*Department of Chemical Engineering, Indian Institute of Technology Hyderabad, Kandi,
Sangareddy, Telengana 502284, India*

Abstract

Controlling flow-induced segregation in a granular mixture is highly relevant to many industrial settings. To enhance mixing or promote segregation, the continuous gravity flow of a bidisperse granular mixture through a series of narrow vertical channels with exit slots is investigated. The bidisperse mixture is composed of two different sizes of particles, but of the same density. In dense flow, segregation occurs, leading to formation of bands. The bands of large particles appear at a distance away from the walls. This finding is in contrast to that in shear-driven segregation in a dense flow where large particles segregate towards the walls. Using a phenomenological model, it has been shown that rolling and bouncing induced segregation is the dominant mechanism. When cylindrical inserts are placed to modify flow patterns, that significantly influences segregation patterns. The symmetrical placement of a cylindrical insert close to the exit slot vanishes the bands and enhances mixing. However, with two inserts placed symmetrically and close to the exit slot, the degree of segregation in the reverse direction is greatly enhanced compared to that without insert. In the former,

^{*}To whom correspondence must be addressed: bhanjan@che.iith.ac.in

small particles accumulate in thin regions adjacent to the walls, and large particles comprise the bulk of the domain and the flowing stream. The heap formation above the insert in a narrow channel, when the insert is close to the exit, enhances mixing in one configuration, whereas it amplifies reverse segregation in the other.

1 Introduction

Granular mixing and segregation are two important unit operations frequently encountered in the powder and grain industries (Ottino & Khakhar, 2001; Rao & Nott, 2008; Bridgwater, 2012). It has long been known that granular mixtures constituted by particles of different sizes, densities, or surface properties segregate under conditions, such as external vibration or shear (Ahmad & Smalley, 1973; Gray & Hutter, 1997; Shinbrot & Muzzio, 1998; Ottino & Khakhar, 2000; Johnson *et al.*, 2012). Extensive research has been conducted on segregation in various flow configurations, including free surface flow inside a rotating tumbler (Das Gupta *et al.*, 1991; McCarthy *et al.*, 1996; Gray, 2001; Jain *et al.*, 2005), flow over an inclined chute (Khakhar *et al.*, 1999b; Wiederseiner *et al.*, 2011; Tripathi & Khakhar, 2013), bounded heap flow (Fan *et al.*, 2012, 2017), flow inside cylindrical Couette geometries (Hill & Fan, 2008; Golick & Daniels, 2009), and flow through a silo (Artega & Tüzün, 1990; Samadani *et al.*, 1999; Ketterhagen *et al.*, 2008). In flow-induced segregation, the pressure gradient induced by the gravity and the gradient of the shear rate can be dominant to influence segregation (Khakhar *et al.*, 1999a; Gray & Thornton, 2005; Fan & Hill, 2011b; Umbanhowar *et al.*, 2019; Jing *et al.*, 2022; Sahu *et al.*, 2023; Duan *et al.*, 2024). It has been shown that the interplay among an advective flow field, diffusion due to grain temperature and percolation determines mixing and segregation (Khakhar *et al.*, 1997; Fan *et al.*, 2014). Despite a deep understanding, less is explored how segregation can be controlled in a flow configuration under the same operating conditions, such as the effect of overburden and the mass flow rate. To address this former issue, one possible mechanism

can be the use of flow-modifying inserts (Cliff *et al.*, 2021; Irvine *et al.*, 2023).

Since many decades, flow of grains past inserts or obstacles was investigated (Wiegardt, 1975; Tüzün & Nedderman, 1985*a,b*; Tardos *et al.*, 1998; Chehata *et al.*, 2003; Gravish *et al.*, 2014; Agarwal *et al.*, 2021). An important aspect in such flows is to design inserts based on the forces (drag and lift) they encounter, and how the flow dynamics influence these forces (Ding *et al.*, 2011; Guillard *et al.*, 2014; Debnath *et al.*, 2017; Dhiman *et al.*, 2020). However, there is a little progress in this area of granular flow due to their complex rheology and the lack of a suitable constitutive law (Debnath *et al.*, 2022*a*). Numerous studies showed complex flow patterns and regimes in simple flow configurations that existing theories do not capture (Krishnaraj & Nott, 2016; Bharathraj & Kumaran, 2019; Dsouza & Nott, 2021; Debnath *et al.*, 2022*b*, 2023). Furthermore, mixing and segregation are complex processes. The coupling between the flow dynamics and segregation is not straightforward even in simple flow configurations (Guillard *et al.*, 2016; Jing *et al.*, 2022; Yennemadi & Khakhar, 2023; Liu *et al.*, 2023). Because of these reasons, segregation in flow past an insert is less investigated.

In flow past an insert, a dense stagnant zone and shock wave arise in the upstream and a grain-free wake zone appears in the downstream. The sizes of the stagnant zone and the wake zone depend on the upstream velocity, the shape of the insert, and distances of the free surface and the exit slot from the insert (Wassgren *et al.*, 2003; Cui & Gray, 2013; Mathews *et al.*, 2022; Tregaskis *et al.*, 2022). If the insert is cylindrical, the size of the wake zone reduces, adopting a triangular shape as the upstream velocity decreases (Chehata *et al.*, 2003; Cui & Gray, 2013; Chen *et al.*, 2022; Tregaskis *et al.*, 2022). There is an interesting observation related to the stagnant zone. A recent work (Mathews *et al.*, 2022) showed that the stagnant zone takes the shape of a stable heap due to a continuous flow. It dissolves in absence of the flow. The height of the heap is a function of the diameter of the cylinder and strongly depends on the solids fraction. However, it shows weak dependence on the grain diameter and the upstream velocity. In a dense flow, the maximum height of the heap is approximately the diameter of the cylinder.

It can be speculated that if the cylinder’s diameter is comparable to the flow dimensions in a bounded dense flow, such heap formation can significantly alter the surrounding flow patterns. Therefore, it raises a question: can the extent of segregation be controlled by modifying the flow patterns in a bounded dense flow using cylindrical inserts?

Here we investigate a continuous flow through a series of narrow vertical channels with exit slots. The cylindrical inserts of diameter comparable to the narrow dimension of the channel are placed inside the bed at different locations to modify the flow patterns. We adopt a simulation based approach using the discrete element method (DEM) to simulate the flow. We observe that without insert, large particles segregate away from the wall regions, in contrast to the outcome in a purely shear-driven process (Fan & Hill, 2011a). In the latter, large particles segregate towards the walls in a dense flow. Our phenomenological model reveals that rolling and bouncing induced segregation due to the free surface at the top is the dominant mechanism. The model explains how this mechanism drives large particles away from the walls in a narrow channel, which is different from free surface segregation (Fan *et al.*, 2017). By placing inserts, we demonstrate that the degree of segregation can be controlled in a narrow channel. We show that the degree of segregation of large particles towards the central region is further enhanced when two inserts are placed symmetrically close to the exit slot, whereas the symmetrical placement of an insert near the exit slot reduces the degree of segregation. We present the details of the configurations with inserts and the DEM simulation in section 2, and report the results in section 3 with a discussion and future scopes in section 4.

2 Flow configurations and DEM simulation

The discrete element method (DEM) is used to simulate the continuous gravity flow through a series of vertical channels (figure 1). The dimensions of one channel are $2W \times H \times B$ in the x -, y - and z - directions, respectively. Instead of simulating flow

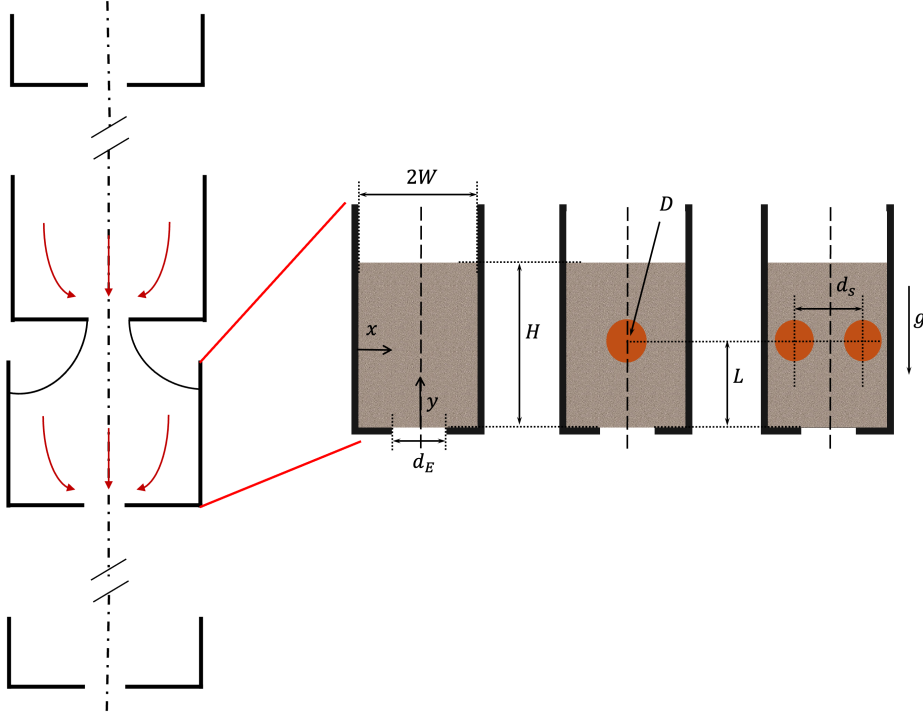


Figure 1: The first panel is the schematic of gravity flow through a series of vertical channels. The other panels represent schematics of one channel without and with inserts (of diameter D) at different locations.

through a series of channels, we employ periodic boundary conditions in the flow (y -) and vorticity z - directions to avoid simulating large number of particles. The flow is bounded by two flat frictional walls at a distance $2W$. To control the flow in the y -direction, there is a flat bottom with an exit slot of width d_E .

To prepare the granular column, the exit slot is closed and the simulation box is filled with particles by uniformly pouring them from the top. The particles are spherical and of two different diameter d_p and $d_p/2$. Here d_p is denoted as the nominal particle diameter. Approx. 10^5 particles are poured with number fraction 1:1 for d_p and $d_p/2$. As the particle density is the same for both large and small particles, it implies that the mass ratio of large to small particles is 8:1. After the particles settle under gravity, the height of the static bed attained is $H^* \sim 50 d_p$ for $2W = 50 d_p$ and $B = 20 d_p$. To initiate the flow, the exit slot of width $d_E = 10 d_p$ is opened, H is set to $60 d_p$, and the periodic boundary conditions are imposed in the y - and z - directions.

To investigate the role of inserts, two new configurations are generated where cylindrical inserts are placed at a height L from the bottom of the channel:

1. one insert with its axis parallel to the z - direction is placed symmetrically with respect to the central plane of the channel (figure 1),
2. two inserts with their axes parallel to the z - direction are placed symmetrically with respect to the central plane of the channel (figure 1). The symmetrical placement of two inserts yields to a center-to-center distance $d_s = W$.

In both configurations, the inserts are kept stationary. The diameter of the insert is D and its length is equal to the depth B . The outer surface of an insert is roughened by coating it with rigid spherical particles of diameter d_p arranged in close-packed hexagonal lattice. To place an insert inside the channel, particles are removed from the cylindrical region of dimensions $0.5 d_p$ greater than the dimensions of the insert to avoid overlap between insert-particles and surrounding active particles.

In the present work, we focus on inserts influencing mixing and segregation in a vertical channel under the same operating conditions such as the overburden and the mass flow rate. That's why, we do not vary the initial filled height H^* , $2W$, B and d_E . The only parameters left are D and L . At present, we fix the value of $D = 15 d_p$ and report the results for three values of $L = 15 d_p$, $30 d_p$, and $45 d_p$.

The linear spring-dashpot contact force model is used to simulate particle–particle, particle–wall, and particle–insert interactions. In all interactions, the model parameters such as the spring constants (k_n, k_t) , damping constants (ξ_n, ξ_t) , and coefficient of friction (μ_p) are set the same. The details of the DEM and values of the model parameters are described in our earlier work (Debnath *et al.*, 2022*a,b*). The length is scaled by d_p , time by $\sqrt{d_p/g}$, velocity by $\sqrt{g d_p}$, force by $\rho_p g d_p^3$, and stresses by $\rho_p g d_p$. Without loss of generality, d_p , ρ_p and g can be set to 1. To perform spatial averaging of the flow properties locally, the simulation box is divided into bins of dimensions $2 d_p \times 2 d_p$ in the x - and y - directions which span the depth B in the z - direction.

3 Results

In the present work, the number fraction will provide an estimate of the extent of segregation. For example, the number fraction n_f^l of large particles is defined as the ratio of the number of large particles to the total number of particles in an averaging bin. Note that the flow configuration is a flat-bottomed bin with an exit slot. To generate a continuous flow, the simulation box dimension in the flow y - direction is chosen higher than the height of the static bed. Therefore, the formation of a free surface at the top and stagnant zones at the corners of the bottom cannot be avoided in the flow configurations investigated here. The average solids fraction in the flowing state is $\bar{\phi} \sim 0.59$.

3.1 With no insert

Figure 2a shows the number fraction distribution of large particles (n_f^l) at different times. Initially, the mixture is almost uniform. The average solids fraction, which is the ratio of the volume of all particles to the volume of the region in the channel that the material occupies, is significantly higher ($\bar{\phi} \sim 0.59$), indicating a dense flow. As time progresses, segregation occurs and bands of large particles appear in regions offset to the central zone and the walls. The central zone and the stagnant zones remain less affected by segregation. The material in the central zone moves as a plug except close the free surface and the exit slot, and the velocities are negligible in the stagnant zones (figure 2b). At a steady state, a striking observation is that small particles accumulate near the walls. There are concentrated layers of small particles moving slowly close to the walls and just above the stagnant zones (figures 2a,b). It appears that the small particles are forming an interface between the stagnant zone and the flowing zone close to the exit slot. These observations are opposite to that in shear-driven segregation.

Size segregation in a vertical channel has been shown to be a shear-driven process [Fan & Hill \(2011a\)](#). In the former, large particles accumulate near the walls and small particles between the central zone and the walls in dense flows when $\bar{\phi}$ is high. In

contrast, this trend reverses when the material is loose under dilute flow conditions, with large particles segregating towards the center of the channel [Fan & Hill \(2011a\)](#). In another context, if there is an inclined free surface at the top (see figure 2b), it can increase the probability of accumulation of large particles near the walls ([Samadani et al., 1999](#); [Fan et al., 2012](#)). However, the bands of large particles appear at a distance away from the walls in the present flow configuration (figure 2a). This raises the question: which effect dominates the shear and the free surface flow, leading to the opposite trend in a dense flow configuration?

We hypothesize that rolling and bouncing motion of particles above the free surface can affect segregation trends in the following manner. The particles escaping the inlet stream hit the free surface and bounce. Small particles are more likely to bounce more and can reach the walls in a narrow channel, whereas large particles tend to roll over the free surface. If large particles stop in between while rolling before reaching the walls and advect downward with the flowing stream, this mechanism can result in the segregation of large particles away from the walls. Using a phenomenological model, we explain how bouncing and rolling of particles over an inclined free surface can induce reverse segregation.

We assume that there are two flowing layers close to the free surface (see figure 2c): (i) dilute ballistic layer above the free surface where particles are not at sustained contacts, and (ii) relatively dense flowing layer of particles at sustained contacts just below the free surface. In the ballistic layer, particles can bounce or roll over the free surface. We imagine the free surface as a series of stairs with rounded edges, continuously forming and vanishing with the flow. The average height and width of the stairs are equivalent to the size of the particles. Assuming the ballistic layer to be very dilute, we can consider the motion of individual particles above these stairs.

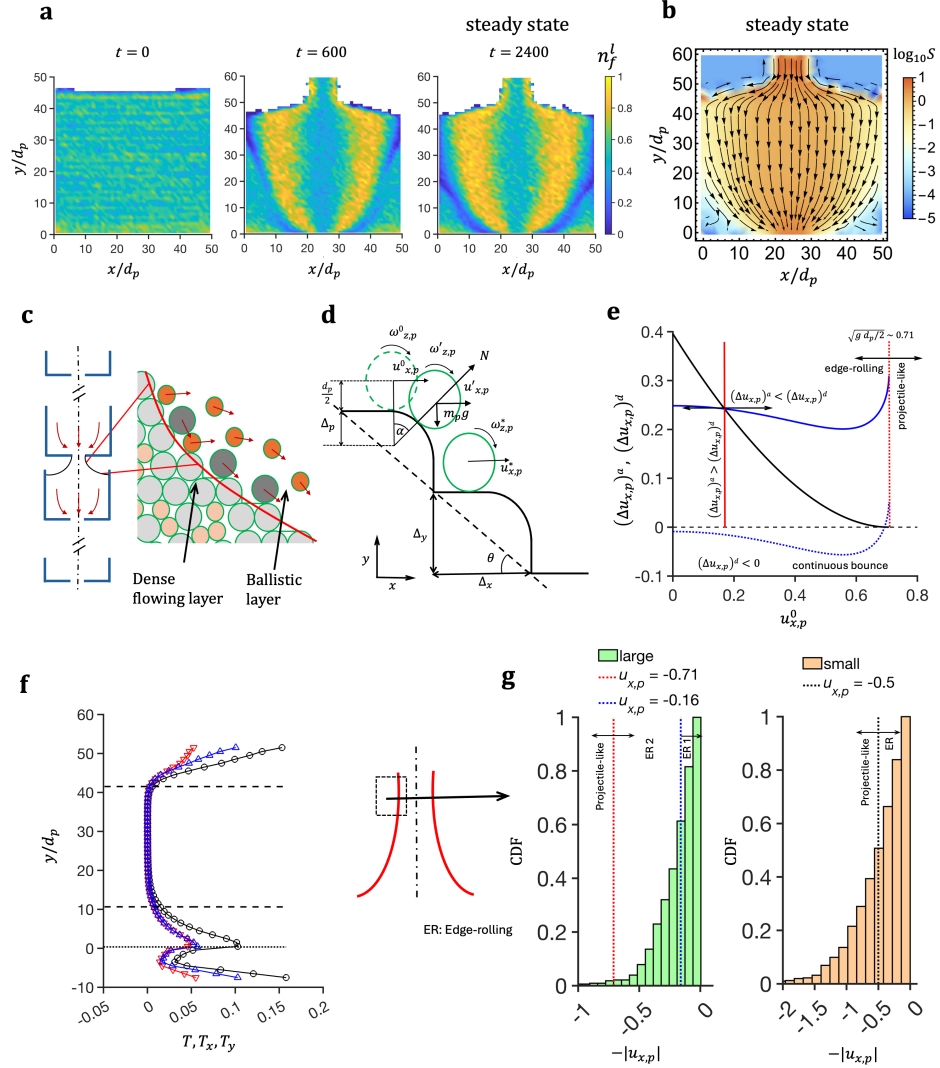


Figure 2: With no insert: (a) The spatial distribution of large particles at different time points. The background color represents the number fraction n_f^l of large particles. (b) Streamlines of the flow at steady state. The background color represents the value $\log_{10} S$, where $S = (u_x^2 + u_y^2)^{1/2}$ is the magnitude of the flow. (c) Schematic of particles rolling and bouncing over the free surface. (d) Schematic of the mechanism of single particle rolling over stairs. (e) The increment $(\Delta u_{x,p})^a$ and decrease $(\Delta u_{x,p})^d$ in the horizontal velocity as functions of $u_{x,p}^0$ due to the acceleration and deceleration processes, respectively. The black curve represents $(\Delta u_{x,p})^a$, and the blue curves represent $(\Delta u_{x,p})^d$. The blue solid curve is for $\theta = 12^\circ$ and the blue dotted curve for $\theta = 30^\circ$. (f) Variation of the granular temperature with the vertical direction y - at the mid-plane of the channel. The black, red, and blue curves represent T , T_x , and T_y , respectively. (g) The cumulative density function (CDF) of the horizontal velocity of individual particles (small and large) leaving from the left edge of the feed stream.

3.1.1 Rolling and bouncing motion of a particle over stairs with rounded edges

For the sake of simplicity, the two dimensional motion of one particle of diameter d_p and mass m_p above the stairs with rounded edges is considered (see figure 2d). We adapted the model of Yan *et al.* (2007), which is for a viscous ball rolling down stairs, and modified it for our system. The particle moves forward due to its initial horizontal velocity. We assume pure rolling and neglect sliding. The particle gains acceleration when it rolls over a rounded edge. The particle can bounce for a while when it hits the next horizontal surface and dissipate its vertical velocity. This effect has not been considered in the model of Yan *et al.* (2007). The particle then experiences deceleration while rolling over the horizontal surface before reaching the next edge. The competition between these two contributions determines whether the particle moves with a constant velocity or stop after traversing a distance.

We will derive the increment in the velocity due to the acceleration process when a particle rolls over an edge (see figure 2d). Consider the particle starts rolling over a rounded edge with horizontal velocity $u_{x,p}^0$ and angular velocity $\omega_{z,p}^0$. When the particle reaches an angle α being at contact with the edge, u'_p and $\omega'_{z,p}$ are its translational and angular velocities. The energy balance of the particle reads as

$$\frac{1}{2} m_p [u_{x,p}^0]^2 + \frac{1}{2} I_p [\omega_{z,p}^0]^2 = \frac{1}{2} m_p [u'_p]^2 + \frac{1}{2} I_p [\omega'_{z,p}]^2 - m_p g \left(\frac{d_p}{2} + \Delta_p \right) (1 - \cos \alpha) + D_r. \quad (1)$$

Here g is the gravitational acceleration, Δ_p represents a distance (see figure 2d), and D_r is the energy dissipated due to rolling friction (Tabor, 1955). We will discuss the contribution of D_r in a short while. Using (1), the assumption of pure rolling, and $I_p = (2/5) m_p (d_p/2)^2$, we can show that the particle velocity u'_p in the limit $\Delta_p \ll d_p/2$ is

$$[u'_p]^2 = [u_{x,p}^0]^2 + \frac{10}{7} g \frac{d_p}{2} (1 - \cos \alpha) - \frac{10}{7} \frac{D_r}{m_p}. \quad (2)$$

When the particle is at the edge, the force balance in the normal and tangential direc-

tions, and the torque balance at the point of contact are, respectively,

$$N - m_p g \cos \alpha + m_p \frac{[u'_p]^2}{d_p/2} = 0; \quad m_p \frac{du'_p}{dt} = -T_r; \quad I_p \frac{d\omega'_{z,p}}{dt} = T_r \frac{d_p}{2} - M_r, \quad (3)$$

where T_r is the tangential force opposite to the direction of motion, and $M_r = \mu_r u'_p N$ (Brilliantov & Pöschel, 1998) is the rolling friction torque, where μ_r is the coefficient of rolling friction. It is reasonable to assume that the dissipation $D_r \leq T_r (\pi d_p/4)$, where the particle over the circular edge can travel a maximum distance equal to one-quarter of the perimeter of the circular edge before it loses contact with the edge. The diameter of the circular edge is d_p , as the rounded edge consists of particles with diameter d_p . For the case of pure rolling and using (3), it can be shown that

$$\frac{10}{7} \frac{D_r}{m_p} \leq \frac{50}{343} \pi d_p \mu_r u'_p \left[g \cos \alpha - \frac{[u'_p]^2}{d_p/2} \right], \quad (4)$$

Brilliantov & Pöschel (1998) showed that the value of $\mu_r = 10^{-6}$ s is very small for a steel ball rolling on a flat non-corrugated surface. Treating the rounded edge in the current problem as equivalent to a flat surface, the third term on the right-hand side of (2) appears to be negligible due to (4). Therefore, in the subsequent steps of the analysis, we neglect the term $(10/7) (D_r/m_p)$ in (2).

When the particle leaves the edge at an angle $\alpha = \alpha_c$, the normal force $N = 0$. Using (2) (neglecting $(10/7) (D_r/m_p)$) and (3), the value of $(\cos \alpha_c)$ and the particle velocity $[u'_p]_c$ after losing contact with the edge can be obtained as

$$\cos \alpha_c = \left(\frac{7 [u_{x,p}^0]^2}{17 \frac{d_p}{2} g} + \frac{10}{17} \right), \quad (5)$$

$$[u'_p]_c^2 = \frac{1}{17} \left(7 [u_{x,p}^0]^2 + 10 \frac{d_p}{2} g \right). \quad (6)$$

Here (5) implies that $u_{x,p}^0 < (g d_p/2)^{1/2}$. If $u_{x,p}^0 \geq (g d_p/2)^{1/2}$, the particle does not roll over the edge. It leaves the edge as a projectile, bounces and rolls on horizontal

surfaces of the stairs. After cycles of energy dissipation through bouncing and rolling, the horizontal velocity eventually decreases to $< (g d_p/2)^{1/2}$. Setting $d_p = 1$ and $g = 1$, the maximum value of $u_{x,p}^0$ below which the particle rolls over the edges is $(g d_p/2)^{1/2} \sim 0.71$.

Therefore, $u_{x,p}^0 = (g d_p/2)^{1/2} = 0.71$ marks the boundary between two regimes of edge-rolling and projectile-like motions. Now, we consider $u_{x,p}^0 < (g d_p/2)^{1/2}$, and analyze the scenario of the particle landing on the next stair after rolling over an edge.

When the particle lands on the horizontal surface, it can bounce due to its non-zero vertical velocity for a short period of time. Upon bouncing, it would not be in continuous contact with the horizontal surface. The particle dissipates its vertical velocity after a few subsequent bounces due to inelastic collisions. We assume that the collisions during bouncing are not oblique, which may not be valid in the current scenario. However, to avoid complexities in the formulation, we neglect the effects of oblique impacts, for example, dissipation of the horizontal and angular velocities.

The vertical velocity reduces to $u_{y,p}^*|_n = (e_p)^n [u'_{y,p}]_c$ after subsequent bounces n , where e_p is the coefficient of restitution. The horizontal distance ℓ_b that the particle traverses while dissipating its vertical velocity is

$$\ell_b = \sum_{n=0}^{\infty} [u'_{x,p}]_c \frac{2 (e_p)^n [u'_{y,p}]_c}{g}, \quad (7)$$

where $[u'_{x,p}]_c = [u'_p]_c \cos \alpha_c$ and $[u'_{y,p}]_c = [u'_p]_c \sin \alpha_c$. As $e_p < 1$, (7) is a geometric series which reduces to

$$\ell_b = \frac{([u'_p]_c)^2 \sin(2\alpha_c)}{g(1 - e_p)}. \quad (8)$$

The distance $\ell_b \rightarrow 0$ for $\alpha_c \rightarrow 0$, irrespective of e_p .

When the vertical velocity dissipates completely, the particle starts rolling over the horizontal surface with horizontal and angular velocities $u_{x,p}^*$ and $\omega_{z,p}^*$, respectively.

When the vertical velocity is negligible, the energy balance can be written as

$$\frac{1}{2} m_p [u'_{x,p}]_c^2 + \frac{1}{2} I_p [\omega'_{z,p}]_c^2 \approx \frac{1}{2} m_p [u^*_{x,p}]^2 + \frac{1}{2} I_p [\omega^*_{z,p}]^2. \quad (9)$$

Neglecting sliding friction, assuming pure rolling and using (9), it can be shown that

$$[u^*_{x,p}]^2 = \frac{5}{7} [u'_{x,p}]_c^2 + \frac{2}{7} [u'_p]_c^2, \quad (10)$$

where $[u'_{x,p}]_c = [u'_p]_c \cos \alpha_c$. Therefore, we can define an increment function for the horizontal velocity as (and using (5) and (6))

$$(\Delta u_{x,p})^a = u^*_{x,p} - u^0_{x,p} = \left(\frac{7[u_{x,p}^0]^2 + 10 \frac{d_p}{2} g}{17} \right)^{1/2} \left(\frac{5 \cos^2 \alpha_c + 2}{7} \right)^{1/2} - u^0_{x,p}. \quad (11)$$

Note that (11) is a function of $u^0_{x,p}$. The increment $(\Delta u_{x,p})^a$ is plotted in figure 2e as a function of $u^0_{x,p}$.

Now, we will discuss the decrease in the horizontal velocity. As mentioned earlier, $u^*_{x,p}$ must decrease due to the rolling friction (Tabor, 1955) as the particle rolls over the horizontal surface towards the next edge (see figure 2d). Using the rolling friction torque $M = (\mu_r u^*_{x,p} m_p g)$ (Brilliantov & Pöschel, 1998), assuming pure rolling, neglecting sliding friction, and using the balances of torques and forces, it can be shown that

$$[u^*_{x,p}]^d(t) = u^*_{x,p} \exp\left(-\frac{5}{7} \frac{\mu_r g}{d_p/2} t\right). \quad (12)$$

As (12) is an exponential function, we can define the decrease in the horizontal velocity due to the deceleration process as

$$(\Delta u_{x,p})^d = \left(\frac{5}{7} \frac{\mu_r g}{d_p/2}\right) \ell_x, \quad (13)$$

where $\ell_x = f(\Delta_y, \Delta_x, \ell_b, u^0_{x,p})$ is the distance that the particle rolls over the horizontal surface, and Δ_y and Δ_x are the heights and breadths of the stairs, respectively.

The value of Δ_y is crucial. If $\Delta_y \leq (d_p/2)(1 - \cos \alpha_c)$, the particle touches the horizontal surface before leaving the edge, and the dynamics would be completely different. It is difficult to comment on the minimum value of Δ_y , as it would depend on the local arrangement of stair-particles. We assume a hexagonal arrangement and set $\Delta_y = \sqrt{3}d_p/2$, which is higher than $d_p/2$. Therefore, the issue of particle touching the horizontal surface before leaving the edge would not be relevant here. The value of $\Delta_x = \Delta_y/\tan \theta$, where θ is the angle of inclination of the free surface. Therefore, the value of ℓ_x would be

$$\ell_x = \Delta_x - \left[\frac{d_p}{2} \sin \alpha_c + \frac{[u'_{x,p}]_c \left(\sqrt{[u'_{y,p}]_c^2 + 2g\ell_y} - [u'_{y,p}]_c \right)}{g} \right] - \ell_b, \quad (14)$$

where $\ell_y = \Delta_y - (d_p/2)(1 - \cos \alpha_c)$, $[u'_{x,p}]_c = [u'_p]_c \cos \alpha_c$ and $[u'_{y,p}]_c = [u'_p]_c \sin \alpha_c$. On the right-hand side of (14), the second term inside the square brackets corresponds to the horizontal distance the particle travels before landing, and the description of the third term ℓ_b in (14) has been provided earlier (see (8)). The former mechanism would be valid only for $\ell_x > 0$. If $\ell_x \leq 0$, then $(\Delta u_{x,p})^d < 0$, which is unacceptable, implying a continuous bouncing motion of the particle.

The function $(\Delta u_{x,p})^d$ in (13) is plotted in figure 2e (blue curves) for two different values of $\theta = 12^\circ$ and 30° , setting $\Delta_y = \sqrt{3}d_p/2$, $\mu_r = 0.07$ s and $e_p = 0.7$. The choice of Δ_y has been discussed earlier. A large value of μ_r is expected for a spherical particle interacting with a bumpy-frictional surface or a nearly spherical/irregular-shaped particle interacting with a flat-frictional surface (Wensrich & Katterfeld, 2012; Cross, 2015; Zhang *et al.*, 2018; Tripathi *et al.*, 2021). For $\theta = 12^\circ$, $(\Delta u_{x,p})^d > 0$ and $(\Delta u_{x,p})^d$ intersects $(\Delta u_{x,p})^a$. For a higher angle of inclination $\theta = 30^\circ$ and $(\Delta u_{x,p})^d < 0$, a particle bounces continuously. Therefore, there are four regimes (figure 2e):

1. Edge-rolling regime 1: In this regime, $u_{x,p}^0 < (gd_p/2)^{1/2} \sim 0.71$ and $(\Delta u_{x,p})^d \leq (\Delta u_{x,p})^a$. The left of the intersection point in figure 2e implies continuous rolling motion of the particle over the stairs.

2. Edge-rolling regime 2: In this regime, $u_{x,p}^0 < (g d_p/2)^{1/2} \sim 0.71$ and $(\Delta u_{x,p})^d > (\Delta u_{x,p})^a$. The right of the intersection point in figure 2e implies that the particle rolls over the stairs, but it stops after traversing a distance.
3. Projectile-like regime: In this regime, $u_{x,p}^0 \geq (g d_p/2)^{1/2} \sim 0.71$. The particle leaves stair-edges as a projectile and after subsequent bounces, its motion falls under the edge-rolling regimes.
4. Continuous bounce: In this regime ($\ell_x \leq 0$), the particle bounces continuously and never falls under the edge-rolling regimes.

These regimes explain the reverse segregation pattern shown in figure 2a as follows.

3.1.2 Model explains how bouncing and rolling induce reverse segregation

The central zone remains less effected by segregation, and the granular temperature is negligible in this zone (between two black dashed horizontal lines in figure 2f). The granular temperature is a measure of the velocity fluctuations, defined as $T = T_x + T_y + T_z$, where $T_x = (u'_x)^2/3$, $T_y = (u'_y)^2/3$, and $T_z = (u'_z)^2/3$ are the contributions of the velocity fluctuations in the x -, y -, and z - directions, respectively (Debnath *et al.*, 2024). However, near the exit location and the feed stream, T is not negligible (figure 2f). (Note that the zone in the negative y in figure 2f represents the part of the feed stream due to the periodic boundary in the y - direction). Due to the converging flow near the exit slot, T_x is comparable to T_y (figures 2b,f). The former implies that the horizontal velocity of the individual particles is not negligible in the exit location and the feed stream. As T is high at the feed stream location and the feed stream has traction-free edges, particles can escape from these edges. Those particles leaving the edges either roll down or bounce over the free surface. Then, this scenario is equivalent to what has been discussed in the previous sub-section 3.1.1.

During the onset of segregation between time points $t = 3$ and $t = 600$, the horizontal velocity distributions of individual particles (small and large) that escape from

the left edge of the feed stream are shown in figure 2g. (Because the flow is symmetric, only the left side is shown.) A negligible fraction of large particles of diameter $d_p = 1$ has velocity $< -(g d_p/2)^{1/2} = -0.71$ (figure 2g). Hence, large particles leaving the traction-free surface move by rolling along the free surface and fall under edge-rolling regimes. As the diameter of small particles is $d_p/2 = 1/2$, the critical value above which they escape as projectiles is $(g d_p/4)^{1/2} = 0.5$ (see sub-section 3.1.1). Figure 2g shows that about $\sim 50\%$ of small particles exceed this critical value and, therefore, escape as projectiles. It indicates that small particles are more likely to reach the walls via bouncing motion in a narrow channel. But bouncing alone cannot explain why only small particles accumulate near the walls. Large particles can also reach the walls by rolling over the free surface, which is less likely in the current flow configuration for the following reason.

As mentioned in sub-section 3.1.1, there are two regimes when a particle rolls. In the edge-rolling regime 1, $(\Delta u_{x,p})^d \leq (\Delta u_{x,p})^a$ and a particle rolls down continuously. In the edge-rolling regime 2, $(\Delta u_{x,p})^d > (\Delta u_{x,p})^a$ and a particle stops after traversing a distance. In the current flow configuration, it is observed that $\theta \sim 12^\circ$, for which the boundary between edge-rolling regimes 1 and 2 is marked at $u_{x,p}^0 \sim 0.16$ when $d_p = 1$. The value of $\Delta_x \sim 4 d_p$ for $\Delta_y = \sqrt{3}d_p/2$ and $\theta = 12^\circ$. This value of Δ_x is approximately one-sixth of the half-width W of the channel. For this small value of θ , figures 2e,g show that the motion of about $\sim 60\%$ of large particles falls under the edge-rolling regime 2. Therefore, it is more likely that their motion would arrest after traversing a distance that is a few multiples of Δ_x . This is the reason for accumulation of large particles at a distance offset to the walls. If the time scale of shear-induced segregation with a shear rate $\dot{\gamma}$ is $O(1/\dot{\gamma}) \propto \sqrt{W/g}$, it is higher than the time scale for the free surface flow $\sqrt{(d_E/2)/g}$. The former implies that the accumulated large particles are advected at a faster rate with the downward flowing stream before they experience shear-induced segregation (Fan & Hill, 2011a; Neveu *et al.*, 2022), resulting in reverse segregation pattern as reported in figure 2a.

However, it should not be interpreted that the contribution from shear-induced

segregation is negligible. We state that rolling and bouncing-induced segregation can be the plausible mechanism in the present scenario that can dominate over shear. The value of θ is an important flow-parameter here, and depends on the height of the feed stream and the width of the channel. For a large value of $\theta = 30^\circ$, the probability would be higher for both large and small particles accumulating near the walls in the narrow channel due to continuous bouncing. However, in a wider channel, only large particles are expected to accumulate near the walls, as observed in earlier studies (Fan *et al.*, 2012; Zhang *et al.*, 2018; Isner *et al.*, 2020). The topic of free surface segregation merits more attention to investigate the interplay among the angle of inclination of the free surface θ and the width of the channel W/d_p , and the velocities and fluxes of the particles (leaving from the edges). This forms a part of future work to understand free surface segregation for the current flow configuration.

3.2 With cylindrical inserts

3.2.1 With one insert

The degree of segregation reduces with the depth of the insert from the free surface (figures 3a–f). Rolling and bouncing induced segregation is unavoidable due to the free surface at the top. When the insert is close to the free surface at $L/d_p = 45$, the segregation pattern and downstream flow profile appear similar to that without an insert (figures 3a,b). It is noticeable that the angle of inclination of the free surface near the center of the channel is higher due to the insert. Therefore, large particles can reach the walls via continuous rolling or bouncing, resulting in a minor shift of the bands towards the walls.

When the insert is at an intermediate depth $L/d_p = 30$, bands of large particles shift towards the walls (figure 3c). However, for $L/d_p = 15$, these bands almost disappear (figure 3e). The streamlines in figure 3d indicate that the diversion in the flow from vertical to horizontal is stronger, shifting the segregated bands towards the walls. For $L/d_p = 15$, the flow diversion from vertical to horizontal is not strong enough to

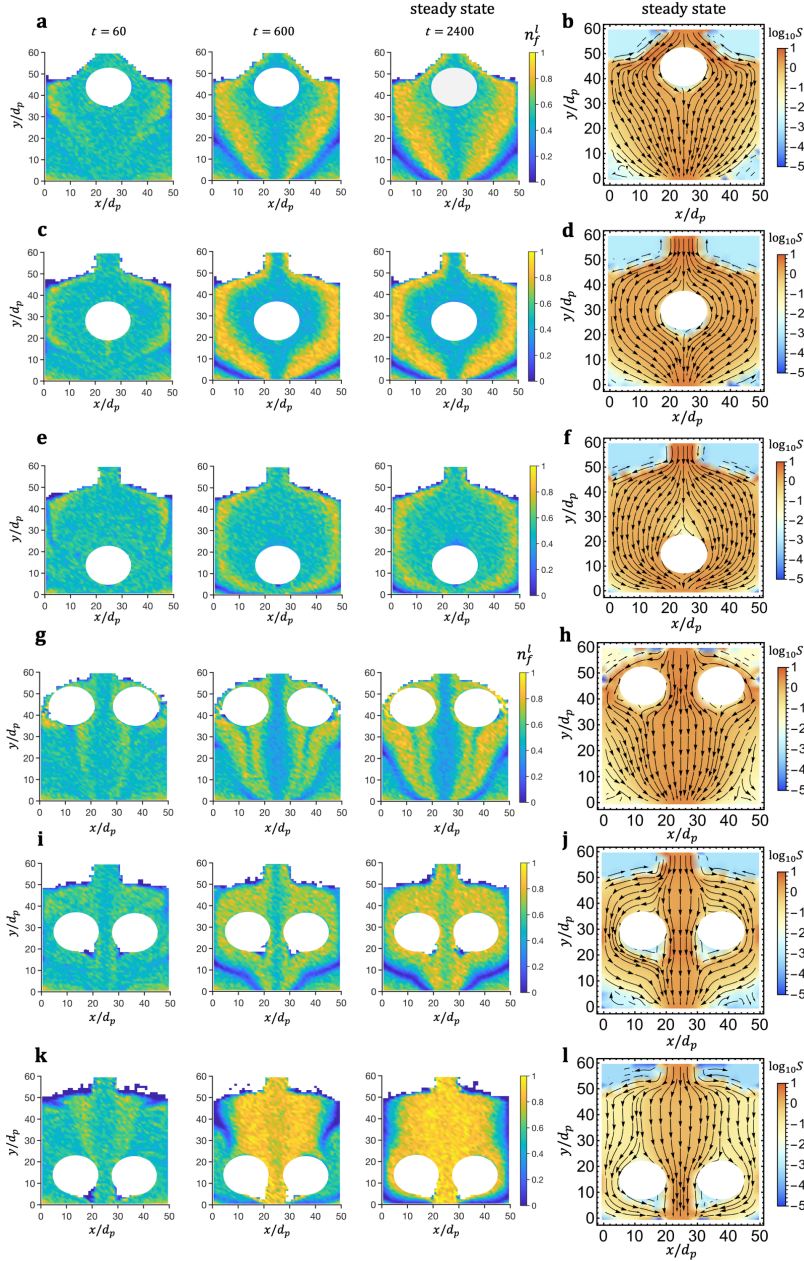


Figure 3: With inserts. The spatial distributions of large particles at different times for one and two inserts at different depths are shown in (a), (c), (e), (g), (i) and (k); the background color represents the number fraction n_f^l of large particles. Streamlines of the flows at steady state are shown in (b), (d), (f), (h), (j) and (l); the background color represents the value $\log_{10} S$, where $S = (u_x^2 + u_y^2)^{1/2}$ is the magnitude of the flow. The profiles in (a)–(f) are for one insert, and (g)–(l) for two inserts. In (a), (b), (g) and (h), $L/d_p = 45$; in (c), (d), (i) and (j), $L/d_p = 30$; in (e), (f), (k) and (l), $L/d_p = 15$.

shift the bands (figure 3f), unlike in $L/d_p = 30$. In $L/d_p = 15$, the vertical velocity u_y gradually decreases to zero above the insert at the mid-plane (figure 4a). (The magnitude of the horizontal velocity is negligible at this plane and is not shown.) This confirms the presence of a heap when the insert is close to the exit slot and no heap formation occurs in other cases. This heap formation is due to the pressure caused by the shock in the upstream region and friction which promote the material to pile above the insert. Such observations have been reported earlier (Gray *et al.*, 2003; Mathews *et al.*, 2022). This flow modification due to the heap is significant, which leads to dissolution of the bands of large particles and stagnant zones (figures 3e,f).

The flow geometry and boundary conditions examined here equivalently represent the flow through a multi-tray vertical column (figure 4e). The tray of interest is far from the trays at the top and bottom of the column. The exit stream from one tray is the inlet of the next tray. The difference in the number fractions between large and small particles, $(n_f^l - n_f^s)$, of the exit zone shown by the green shades in figure 4e has been plotted over time. This quantity implies the extent of segregation; the values $(n_f^l - n_f^s) = 0$ and 1 correspond to well-mixed and purely concentrated state with large particles, respectively. In figure 4f, the profile for $L/d_p = 45$ is closer to the case with no insert. At other heights, the extent of segregation is reduced with a decrease in L/d_p . The trends of $(n_f^l - n_f^s)$ are shown to be well fitted by exponential functions, as explained by using a model in section 3.2.3.

The shear rate $\dot{\gamma}$ and granular temperature T indicate that the gradients are strong in the wall regions when there is no insert and an insert close to the free surface i.e., $L/d_p = 45$ (figures 5a,b,d,e). The difference $(T_y - T_x)$ in the flow direction is also higher in regions where $\dot{\gamma}$ and T are high (figures 5g,h). The quantity $(T_y - T_x)$ is an indirect measure of the degree of anisotropic diffusion, which promotes mixing in certain directions. The gradients in $\dot{\gamma}$ and T weaken when the insert is inside the bed. The flow enhancement due to an insert inside a narrow channel homogenizes the fields around the insert. It is further strengthened when there is a heap above the insert in $L/d_p = 15$. We speculate that the modified flow pattern weakens the anisotropic

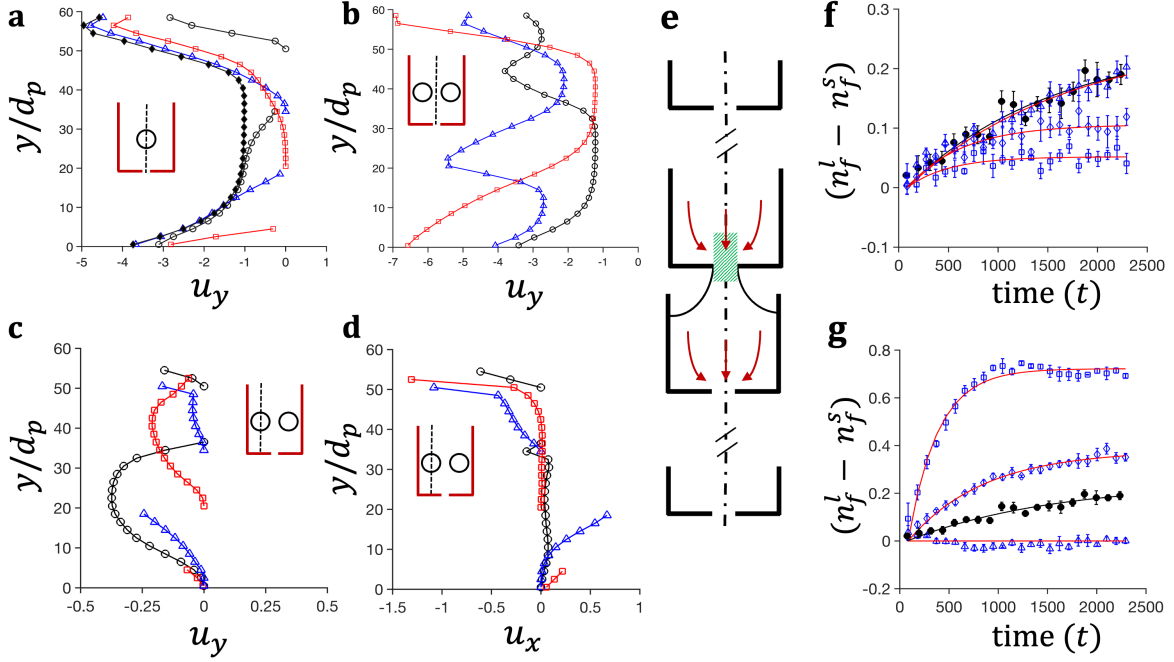


Figure 4: Variation of flow velocity u_y with y/d_p at the mid-plane $x/d_p = 25$ for one insert (a) and two inserts (b). (c) and (d) With two inserts: variation of u_y and u_x with y/d_p at position $x/d_p = 12.5$. In (a), the filled \diamond symbol represents the data for the case–no insert. With one insert and two inserts at different heights in (a)–(d), black \circ , $L/d_p = 45$; blue \triangle , $L/d_p = 30$; red \square , $L/d_p = 15$. The data are shown for the planes marked as vertical lines in the insets. (e) Schematic of a multi-tray vertical tower. Variation of $(n_f^l - n_f^s)$ with time t in the green shaded exit region shown in (e) for the cases of one insert (f) and two inserts (g). In (f) and (g), solid \circ , no insert; \triangle , $L/d_p = 45$; \diamond , $L/d_p = 30$; \square , $L/d_p = 15$. The error bars represent 95% confidence limits of time-averaged values over a period $\Delta t = 125$. The red curves are the fits for the exponential function $y = b(1 - e^{-at})$.

diffusion field around the insert where $\dot{\gamma}$ and T are finite, and reverses the direction of the percolation flux at locations prone to segregation, resulting in enhanced mixing.

3.2.2 With two inserts

In figures 3g,h and figures 5c,f,i, when the inserts are close to the free surface ($L/d_p = 45$), they tend to weaken the formation of strong bands of large particles. The stream that bifurcates above one of the inserts converges laterally and merges downstream, leaving almost no wake zone. Beneath the insert, where two streams rejoin, one stream from the low shear region near the mid-plane brings higher momentum than the stream near the wall. Although $\dot{\gamma}$, T and $(T_y - T_x)$ profiles in the downstream location are almost similar to those without insert (figures 5c,f,i), two counteracting streams with different momenta appear to inhibit strong band formation of large particles. This is in contrast with the cases with no insert or single insert near the free surface.

A striking observation is that the degree of reverse segregation is significantly enhanced compared to all other cases examined here, particularly when the inserts are close to the exit slot at $L/d_p = 15$ (figures 3i-1). To the best of our knowledge, this finding has been reported for the first time. The flow is not symmetric around an insert. It is important to note that the speed of the material is significantly reduced near the wall regions (figures 3j,l). The vertical velocity u_y at the mid-plane is higher than at the plane that passes through the center of the insert (figures 4b,c). At height $L/d_p = 15$, heaps are forming above the inserts, which are absent for $L/d_p = 30$. This is further confirmed by the velocity profiles shown in figures 4c,d. The profiles of u_y and u_x gradually decrease to zero as the flow approaches the inserts in $L/d_p = 15$, while only u_y decreases to zero with non-zero u_x above the inserts in $L/d_p = 30$. The occurrence of slow mobile zones near the walls is reflected in the profiles of $\dot{\gamma}$, T and $(T_y - T_x)$ (figures 5c,f,i). The evolution of $(n_f^l - n_f^s)$ with time reflects the degree of enhanced segregation compared to that when there is no insert and the inserts are close to the free surface (figure 4g) (the reason for exponential trends are discussed in

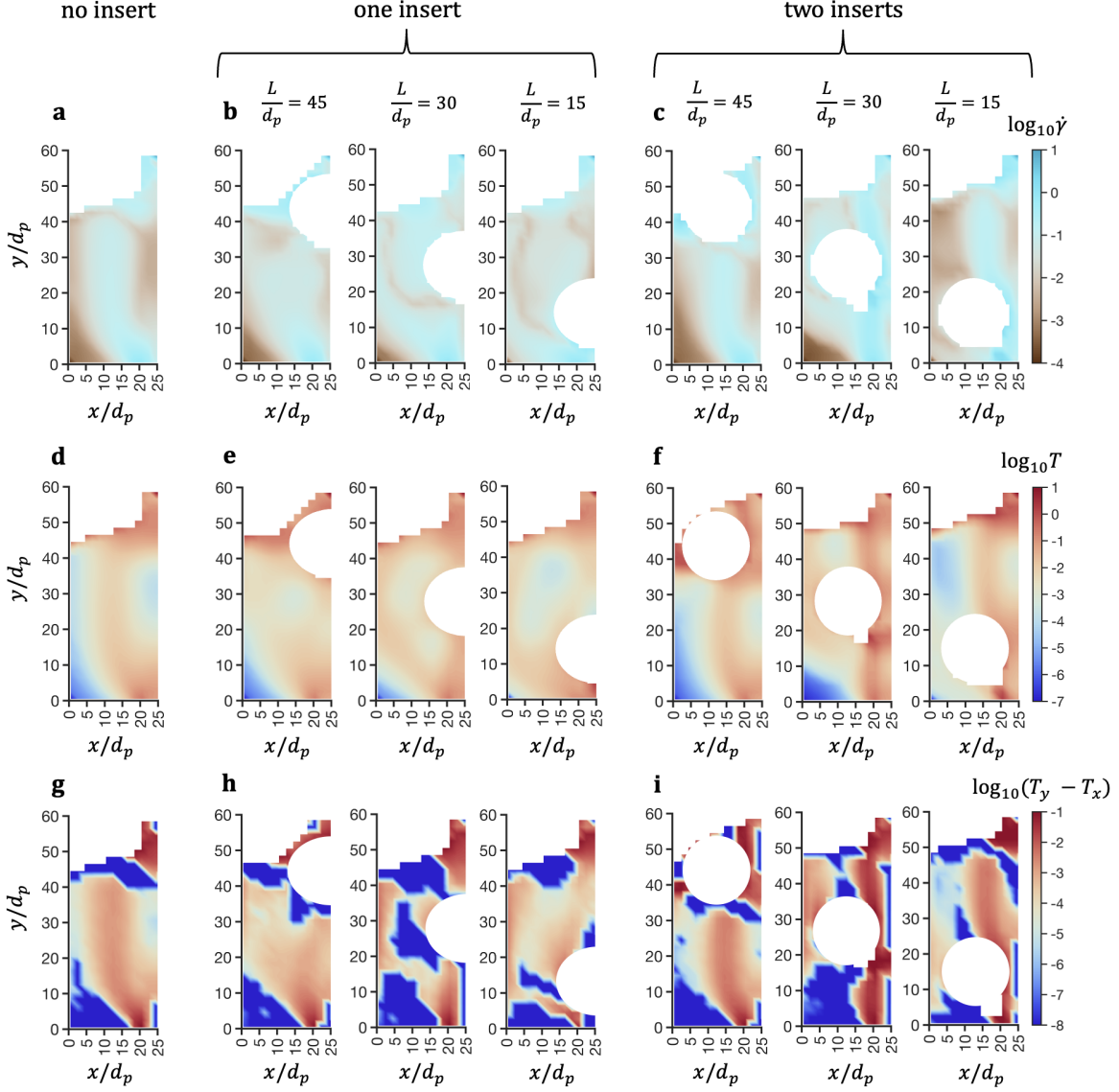


Figure 5: The color maps of the shear rate $\dot{\gamma}$ ((a)–(c)), granular temperature T ((d)–(f)), and difference in temperature ($T_y - T_x$) ((g)–(i)) between x - and y - directions for different cases. The background color represents the $\log_{10}(\star)$ values of the above variables. No insert; (a), (d), (g). With one insert for different values of L/d_p ; (b), (e), (h). With two inserts for different values of L/d_p ; (c), (f), (i).

section 3.2.3). When the streamlines bifurcate above the inserts, the grains following the streamlines close to the wall lose their momentum due to increased frictional dissipation aided by narrow constrictions. The smallest gap for the material to flow in these regions is a few particle diameters that can even cause jamming. This effect is further enhanced due to the formation of heaps in the case $L/d_p = 15$.

In these former cases, segregation due to the rolling and bouncing above the free surface is unpreventable. The small particles leaving the inlet stream reach the walls by bouncing. Their momentum dissipates near the wall regions, causing them to move slowly downward. The resistance to diffuse from the wall regions towards the central region increases as a result of these low-mobility regions, making it nearly impossible for small particles to rejoin the exit stream. As the flow is continuous due to the periodic boundary in the flow direction, small particles are continuously expelled from the inlet stream with negligible feedback in the exit stream. Thus, thin regions near the walls concentrated with small particles. Further the location of heaps in $L/d_p = 15$ appears to bifurcate the stream—one concentrated with small particles slowly moving near the walls and the other with large particles flowing relatively easily in the central zone. This is more likely the reason for enhanced segregation of large particles in the reverse direction towards the central region when inserts are close to the exit slot.

3.2.3 Exponential scaling is explained by using a continuum model

The trends of $(n_f^l - n_f^s)$ are shown to be well fitted by exponential functions (solid red curves in figures 4f,g). The reason for the exponential trends is the following. The time evolution of the number fractions of large (n_f^l) and small (n_f^s) particles are (Fan *et al.*, 2014; Kumawat *et al.*, 2025)

$$\frac{\partial n_f^l}{\partial t} + \nabla \cdot (\mathbf{u} n_f^l) + \nabla \cdot \mathbf{J}_{sg}^l + \nabla \cdot \mathbf{J}_d^l = 0, \quad (15)$$

$$\frac{\partial n_f^s}{\partial t} + \nabla \cdot (\mathbf{u} n_f^s) + \nabla \cdot \mathbf{J}_{sg}^s + \nabla \cdot \mathbf{J}_d^s = 0. \quad (16)$$

Here \mathbf{u} is the velocity of the mixture, and \mathbf{J}_{sg}^l and $\mathbf{J}_d^l = D\nabla n_f^l$ are the segregation and diffusion fluxes, respectively, where D is the diffusivity; superscripts l and s represent large and small particles, respectively. Consider the exit region. Subtracting (16) from (15), and neglecting the variations in the x - direction, except the segregation flux which is assumed to be negligible in the y - direction,

$$\frac{\partial}{\partial t}(n_f^l - n_f^s) = -\frac{\partial}{\partial y} \left[u_y (n_f^l - n_f^s) \right] - \frac{\partial}{\partial x} (J_{sg,x}^l - J_{sg,x}^s) - \frac{\partial}{\partial y} (J_{d,y}^l - J_{d,y}^s). \quad (17)$$

Neglecting the variation of number fractions in the flow (y -) direction, and therefore, omitting the term related to diffusion ($J_{d,y}^l - J_{d,y}^s = D \frac{\partial}{\partial y} (n_f^l - n_f^s) = 0$),

$$\frac{\partial}{\partial t}(n_f^l - n_f^s) = -(n_f^l - n_f^s) \frac{\partial u_y}{\partial y} - \frac{\partial}{\partial x} (J_{sg,x}^l - J_{sg,x}^s). \quad (18)$$

The above (18) is equivalent to

$$\frac{d}{dt}(n_f^l - n_f^s) = -m_1 (n_f^l - n_f^s) + m_2, \quad (19)$$

if $m_1 = \frac{du_y}{dy}$ and $m_2 = -\frac{d}{dx} (J_{sg,x}^l - J_{sg,x}^s)$ are non-zero constants. Therefore, using $(n_f^l - n_f^s) = 0$ at $t = 0$ as the initial condition, (19) yields an exponential function

$$(n_f^l - n_f^s) = \frac{m_2}{m_1} (1 - e^{-m_1 t}), \quad (20)$$

that fits the data well for $m_1 > 0$ and $m_2 > 0$ (red curves in figures 4f,g). If $m_2 = 0$, $(n_f^l - n_f^s) = 0$. The profiles for u_y in the exit region (figures 4a,b) show that the slope is approximately constant and positive. Therefore, to reduce (18) to (19), treating $m_1 > 0$ as a constant is a reasonable assumption. It is difficult to comment *a priori* on whether m_2 would be constant and positive. However, this choice seems to capture the trends satisfactorily.

4 Discussion

Mixing and segregation of granular mixtures are energy intensive processes, for which gravity flow provides efficient solution. Since decades, a variety of gravity flow setups have been engineered based on free-surface and shear-induced segregation mechanisms, enabling control over mixing and segregation through flow parameters such as overburden and flow rate of the material. In this work, we demonstrated that mixing and segregation can be controlled without modifying any flow parameters by introducing flow-modifying inserts and exploiting the confinement effects in a gravity flow setup. By changing number of inserts and their position, we showed significant enhancement in mixing and segregation.

We investigated the flow of bi-disperse material through a narrow vertical channel with an exit slot using DEM simulations. We applied periodic boundary conditions in the flow direction to mimic the flow through a series of bins, and in the vorticity direction. It has been observed that, without any insert, large particles accumulate between the central and wall regions, in contrast to the outcome in a purely shear-driven process (Fan & Hill, 2011a). The central region remains less affected (well-mixed), and the fraction of small particles is higher in the wall regions. Close examination revealed the influence of the free surface on segregation. But, in free surface segregation, it is more likely that large particles accumulate near walls (Samadani *et al.*, 1999). We showed that rolling and bouncing induced segregation followed by downward advection is the dominant mechanism.

Our phenomenological model predicted the existence of multiple regimes. In edge-rolling regime 1, a particle performs a continuous rolling motion, whereas the rolling motion ceases after traversing a distance in edge-rolling regime 2. In the rest of the regimes, a particle performs a projectile-like motion or bounces continuously until it dissipates its kinetic energy subsequently and falls under edge rolling regimes. It has been shown that a large fraction of large particles leaving the inlet stream fall under edge rolling regime 2, whereas small particles perform projectile-like motion or bounce

continuously. This model successfully explained how rolling and bouncing on a low inclined free surface in a narrow column augment the accumulation of small particles in the wall regions and large particles away from the walls. The rolling and bouncing mechanism has been known for some time (Drahn & Bridgwater, 1983; Fan *et al.*, 2012). However, its strong impact on segregation bands has been demonstrated for the first time in a gravity flow with a simple model. More work is required to examine parameters such as the width of the channel and width and height of the inlet stream, to identify the range when the rolling and bouncing mechanism is dominant. This is a separate topic in it-self and forms a part of future work.

With an insert inside the column, the flow pattern changes significantly with an increase in its depth inside the bed. When the insert is close to the free surface, the downstream flow pattern is less affected. The former exhibits a segregation pattern and degree of segregation similar to that without insert. When the insert is away from the free surface and the exit slot, the segregated bands of large particles are advected towards the wall, but a reduction of the degree of segregation in the exit stream. The shift in bands towards walls is due to sharp diversion in the flow. When the insert is close to the exit slot and far away from the free surface, the upstream pressure supports the material piling up above the insert. This is absent in the other cases due to lack of space required for a stable heap formation above the insert. The heap further modifies the flow substantially throughout the domain, and the degree of segregation was found to be further reduced. We hypothesize that the flow modification reverses the percolation flux, which mitigates band formation in segregation-prone regions.

With two inserts, the degree of segregation is significantly enhanced when they are placed inside the column away from the free surface. When the inserts are close to the exit slot, the material piles up above the inserts, leaving the wall regions less mobile in the narrow channel. The material near the wall regions experiences a higher frictional resistance to flow than that in the central region, especially the small particles that accumulate near the walls via rolling and bouncing. The less mobile regions do not support them to migrate from wall regions to the central region and join the

exit stream. The small particles are continuously expelled from the flowing stream, leaving the stream largely constituted by large particles. This leads to enhanced size segregation in the case of two inserts close to the exit slot.

This work leads us to conclude that the cohesionless granular flow around an intruder or obstacle in a narrow channel provides enriching insights into local hydrodynamics and flow-structure interactions. There is a body of work on intruder dynamics. However, it is less often envisaged how such complex interactions can strongly influence material transport mechanisms under confined flow conditions. These findings encourage to design and explore flow-structure interactions in confined dense granular flows to manipulate the material transport mechanisms. In complex flows in complex geometries, it is preferred to use the continuum approach to design and optimize the parameters. We did not rigorously attempt to use the former. While we believe that it will be fruitful to work with a continuum description in such scenarios to resolve complex flow patterns, the challenge may remain to choose or develop a well-posed constitutive theory and suitable boundary conditions for granular flows (Debnath *et al.*, 2022*a*).

Acknowledgements

The author thanks Prof. K. Kesava Rao and Prof. V. Kumaran for valuable discussions. The author acknowledges the support of PARAM PRAVEGA–IISc Bengaluru and PARAM SEVA–IIT Hyderabad under National Supercomputing Mission (NSM) for providing computational support to generate the simulation data. B.D. acknowledges the Department of Science and Technology (DST), Ministry of Science and Technology, India INSPIRE Faculty award DST/INSPIRE/04/2024/000725 for funding.

References

AGARWAL, S, KARSAI, A, GOLDMAN, DI & KAMRIN, K 2021 Surprising simplicity in the modeling of dynamic granular intrusion. *Sci. Adv.* **7**, eabe0631.

- AHMAD, K & SMALLEY, IJ 1973 Observation of particle segregation in vibrated granular systems. *Powder Technol.* **8** (1-2), 69–75.
- ARTEGA, P & TÜZÜN, U 1990 Flow of binary mixtures of equal-density granules in hoppers—size segregation, flowing density and discharge rates. *Chem. Engg. Sci.* **45**, 205–223.
- BHARATHRAJ, S & KUMARAN, V 2019 Cessation of a dense granular flow down an inclined plane. *Phys. Rev. Fluids* **4**, 024301.
- BRIDGWATER, J 2012 Mixing of powders and granular materials by mechanical means—a perspective. *Particuology* **10**, 397–427.
- BRILLIANTOV, NV & PÖSCHEL, T 1998 Rolling friction of a viscous sphere on a hard plane. *Europhys. Lett.* **42**, 511.
- CHEHATA, D, ZENIT, R & WASSGREN, CR 2003 Dense granular flow around an immersed cylinder. *Phys. Fluids* **15**, 1622–1631.
- CHEN, S, FANG, W & SHI, S 2022 Flow characteristics and packing structures of dense granular flow around an immersed cylindrical tube. *Chem. Engg. Sci.* **258**, 117773.
- CLIFF, A, FULLARD, LA, BREARD, ECP, DUFEK, J & DAVIES, CE 2021 Granular size segregation in silos with and without inserts. *Proc. Roy. Soc. A* **477**, 20200242.
- CROSS, R 2015 Effects of surface roughness on rolling friction. *Euro. J. Phys.* **36** (6), 065029.
- CUI, X & GRAY, JMNT 2013 Gravity-driven granular free-surface flow around a circular cylinder. *J. Fluid Mech.* **720**, 314–337.
- DAS GUPTA, SD, KHAKHAR, DV & BHATIA, SK 1991 Axial segregation of particles in a horizontal rotating cylinder. *Chem. Engg. Sci.* **46**, 1513–1517.

- DEBNATH, B, KUMARAN, V & RAO, KK 2024 Dense granular flow through a flat-bottomed silo: Comparison of the dem and continuum models with experiments. *Powder Technol.* **431**, 119036.
- DEBNATH, B, KUMARAN, V & RAO, K KESAVA 2022a Comparison of the compressible class of models and non-local models with the discrete element method for steady fully developed flow of cohesionless granular materials through a vertical channel. *J. Fluid Mech.* **937**, A33.
- DEBNATH, B, RAO, KK & KUMARAN, V 2023 Cross-stream oscillations in the granular flow through a vertical channel. *J. Fluid Mech.* **975**, A10.
- DEBNATH, B, RAO, KK & NOTT, PR 2017 The lift on a disc immersed in a rotating granular bed. *AIChE J.* **63**, 5482–5489.
- DEBNATH, B, RAO, K KESAVA & KUMARAN, V 2022b Different shear regimes in the dense granular flow in a vertical channel. *J. Fluid Mech.* **945**, A25.
- DHIMAN, M, KUMAR, S, REDDY, KA & GUPTA, R 2020 Origin of the long-ranged attraction or repulsion between intruders in a confined granular medium. *J. Fluid Mech.* **886**, A23.
- DING, Y, GRAVISH, N & GOLDMAN, DI 2011 Drag induced lift in granular media. *Phys. Rev. Lett.* **106**, 028001.
- DRAHUN, JA & BRIDGWATER, J 1983 The mechanisms of free surface segregation. *Powder Technol.* **36** (1), 39–53.
- DSOUZA, PV & NOTT, PR 2021 Dilatancy-driven secondary flows in dense granular materials. *J. Fluid Mech.* **914**, A36.
- DUAN, Y, JING, L, UMBANHOWAR, PB, OTTINO, JM & LUEPTOW, RM 2024 General model for segregation forces in flowing granular mixtures. *J. Fluid Mech.* **989**, A17.

- FAN, Y, BOUKERKOUR, Y, BLANC, T, UMBANHOWAR, PB, OTTINO, JM & LUEPTOW, RM 2012 Stratification, segregation, and mixing of granular materials in quasi-two-dimensional bounded heaps. *Physical Review E—Statistical, Nonlinear, and Soft Matter Physics* **86**, 051305.
- FAN, Y & HILL, KM 2011*a* Phase transitions in shear-induced segregation of granular materials. *Phys. Rev. Lett.* **106** (21), 218301.
- FAN, YI & HILL, KM 2011*b* Theory for shear-induced segregation of dense granular mixtures. *New J. Physics* **13**, 095009.
- FAN, Y, JACOB, KV, FREIREICH, B & LUEPTOW, RM 2017 Segregation of granular materials in bounded heap flow: A review. *Powder Technol.* **312**, 67–88.
- FAN, Y, SCHLICK, CP, UMBANHOWAR, PB, OTTINO, JM & LUEPTOW, RM 2014 Modelling size segregation of granular materials: the roles of segregation, advection and diffusion. *J. Fluid Mech.* **741**, 252–279.
- GOLICK, LA & DANIELS, KE 2009 Mixing and segregation rates in sheared granular materials. *Physical Review E—Statistical, Nonlinear, and Soft Matter Physics* **80**, 042301.
- GRAVISH, N, UMBANHOWAR, PB & GOLDMAN, DI 2014 Force and flow at the onset of drag in plowed granular media. *Phys. Rev. E* **89** (4), 042202.
- GRAY, JMNT 2001 Granular flow in partially filled slowly rotating drums. *J. Fluid Mech.* **441**, 1–29.
- GRAY, JMNT & HUTTER, K 1997 Pattern formation in granular avalanches. *Continuum Mechanics and Thermodynamics* **9**, 341–345.
- GRAY, JMNT, TAI, Y-C & NOELLE, S 2003 Shock waves, dead zones and particle-free regions in rapid granular free-surface flows. *J. Fluid Mech.* **491**, 161–181.

- GRAY, JMNT & THORNTON, AR 2005 A theory for particle size segregation in shallow granular free-surface flows. *Proc. Roy. Soc. A: Mathematical, Physical and Engineering Sciences* **461**, 1447–1473.
- GUILLARD, F, FORTERRE, Y & POULIQUEN, O 2014 Lift forces in granular media. *Phys. Fluids* **26**.
- GUILLARD, F, FORTERRE, Y & POULIQUEN, O 2016 Scaling laws for segregation forces in dense sheared granular flows. *J. Fluid Mech.* **807**, R1.
- HILL, KM & FAN, YI 2008 Isolating segregation mechanisms in a split-bottom cell. *Phys. Rev. Lett.* **101**, 088001.
- IRVINE, SK, FULLARD, LA, HOLLAND, DJ, CLARKE, DA, LYNCH, TA & LAGRÉE, PY 2023 The $\mu(i)$ model and extensions applied to granular material in silo with inserts. *arXiv preprint arXiv:2302.12550* .
- ISNER, AB, UMBANHOWAR, PB, OTTINO, JM & LUEPTOW, RM 2020 Axisymmetric granular flow on a bounded conical heap: kinematics and size segregation. *Chem. Engg. Sci.* **217**, 115505.
- JAIN, N, OTTINO, JM & LUEPTOW, RM 2005 Regimes of segregation and mixing in combined size and density granular systems: an experimental study. *Granular Matter* **7**, 69–81.
- JING, L, OTTINO, JM, UMBANHOWAR, PB & LUEPTOW, RM 2022 Drag force in granular shear flows: regimes, scaling laws and implications for segregation. *J. Fluid Mech.* **948**, A24.
- JOHNSON, CG, KOKELAAR, BP, IVERSON, RM, LOGAN, M, LAHUSEN, RG & GRAY, JMNT 2012 Grain-size segregation and levee formation in geophysical mass flows. *Journal of Geophysical Research: Earth Surface* **117** (F1).

- KETTERHAGEN, WR, CURTIS, JS, WASSGREN, CR & HANCOCK, BC 2008 Modeling granular segregation in flow from quasi-three-dimensional, wedge-shaped hoppers. *Powder Technol.* **179**, 126–143.
- KHAKHAR, DV, MCCARTHY, JJ, GILCHRIST, JF & OTTINO, JM 1999a Chaotic mixing of granular materials in two-dimensional tumbling mixers. *Chaos: An Interdisciplinary Journal of Nonlinear Science* **9**, 195–205.
- KHAKHAR, DV, MCCARTHY, JJ & OTTINO, JM 1999b Mixing and segregation of granular materials in chute flows. *Chaos: An Interdisciplinary Journal of Nonlinear Science* **9**, 594–610.
- KHAKHAR, DV, MCCARTHY, JJ, SHINBROT, T & OTTINO, JM 1997 Transverse flow and mixing of granular materials in a rotating cylinder. *Phys. Fluids* **9** (1), 31–43.
- KRISHNARAJ, KP & NOTT, PR 2016 A dilation-driven vortex flow in sheared granular materials explains a rheometric anomaly. *Nat. Commun.* **7**, 10630.
- KUMAWAT, S, SAHU, VK & TRIPATHI, A 2025 Transient segregation of different density granular mixtures. *J. Fluid Mechanics* **1008**, A53.
- LIU, D, SINGH, H & HENANN, DL 2023 Coupled continuum modelling of size segregation driven by shear-strain-rate gradients and flow in dense, bidisperse granular media. *J. Fluid Mech.* **976**, A16.
- MATHEWS, AK, KHAN, A, SHARMA, B, KUMAR, S & KUMAR, R 2022 A numerical investigation of granular shock waves over a circular cylinder using the discrete element method. *J. Fluid Mech.* **936**, A11.
- MCCARTHY, JJ, SHINBROT, T, METCALFE, G, WOLF, JE & OTTINO, JM 1996 Mixing of granular materials in slowly rotated containers. *AIChE Journal* **42**, 3351–3363.

- NEVEU, A, LARCHER, M, DELANNAY, R, JENKINS, JT & VALANCE, A 2022 Particle segregation in inclined high-speed granular flows. *J. Fluid Mech.* **935**, A41.
- OTTINO, JM & KHAKHAR, DV 2000 Mixing and segregation of granular materials. *Ann. Rev. Fluid Mech.* **32**, 55–91.
- OTTINO, JM & KHAKHAR, DV 2001 Fundamental research in heaping, mixing, and segregation of granular materials: challenges and perspectives. *Powder Technol.* **121**, 117–122.
- RAO, KK & NOTT, PR 2008 *An introduction to granular flow*, , vol. 490. Cambridge university press Cambridge.
- SAHU, VK, KUMAWAT, S, AGRAWAL, S & TRIPATHI, A 2023 Particle force-based density segregation theory for multi-component granular mixtures in a periodic chute flow. *J. Fluid Mech.* **956**, A8.
- SAMADANI, A, PRADHAN, A & KUDROLLI, A 1999 Size segregation of granular matter in silo discharges. *Phys. Rev. E* **60** (6), 7203.
- SHINBROT, T & MUZZIO, FJ 1998 Reverse buoyancy in shaken granular beds. *Phys. Rev. Lett.* **81**, 4365.
- TABOR, D 1955 The mechanism of rolling friction ii. the elastic range. *Proc. Roy. Soc. A. Mathematical and Physical Sciences* **229** (1177), 198–220.
- TARDOS, GI, KHAN, MI & SCHAEFFER, DG 1998 Forces on a slowly rotating, rough cylinder in a couette device containing a dry, frictional powder. *Phys. Fluids* **10**, 335–341.
- TREGASKIS, C, JOHNSON, CG, CUI, X & GRAY, JMNT 2022 Subcritical and supercritical granular flow around an obstacle on a rough inclined plane. *J. Fluid Mech.* **933**, A25.

- TRIPATHI, A & KHAKHAR, DV 2013 Density difference-driven segregation in a dense granular flow. *J. Fluid Mech.* **717**, 643–669.
- TRIPATHI, A, KUMAR, V, AGARWAL, A, TRIPATHI, A, BASU, S, CHAKRABARTY, A & NAG, S 2021 Quantitative dem simulation of pellet and sinter particles using rolling friction estimated from image analysis. *Powder Technol.* **380**, 288–302.
- TÜZÜN, U & NEDDERMAN, RM 1985*a* Gravity flow of granular materials round obstacles—i: Investigation of the effects of inserts on flow patterns inside a silo. *Chem. Engg. Sci.* **40**, 325–336.
- TÜZÜN, U & NEDDERMAN, RM 1985*b* Gravity flow of granular materials round obstacles—ii: investigation of the stress profiles at the wall of a silo with inserts. *Chem. Engg. Sci.* **40**, 337–351.
- UMBANHOWAR, PAUL B, LUEPTOW, RICHARD M & OTTINO, JULIO M 2019 Modeling segregation in granular flows. *Ann. Rev. Chemical and Biomolecular Engg.* **10**, 129–153.
- WASSGREN, CR, CORDOVA, JA, ZENIT, R & KARION, A 2003 Dilute granular flow around an immersed cylinder. *Phys. Fluids* **15** (11), 3318–3330.
- WENSRICH, CM & KATTERFELD, A 2012 Rolling friction as a technique for modelling particle shape in dem. *Powder Technol.* **217**, 409–417.
- WIEDERSEINER, S, ANDREINI, N, ÉPELY-CHAUVIN, G, MOSER, G, MONNEREAU, M, GRAY, JMNT & ANCEY, C 2011 Experimental investigation into segregating granular flows down chutes. *Phys. Fluids* **23** (1).
- WIEGHARDT, K 1975 Experiments in granular flow. *Ann. Rev. Fluid Mech.* **7**, 89–114.
- YAN, H, SHI, Q, HUANG, D & SUN, G 2007 Dynamics of a viscous ball rolling down on a rigid staircase. *Physica A: Stat. Mech. Appl.* **374**, 524–532.

YENNEMADI, AV & KHAKHAR, DV 2023 Drag, lift, and buoyancy forces on a single large particle in dense granular flows. *Phys. Rev. Fluids* **8**, 074301.

ZHANG, TF, GAN, JQ, PINSON, D & ZHOU, ZY 2018 Size-induced segregation of granular materials during filling a conical hopper. *Powder Technol.* **340**, 331–343.